Room temperature efficient regeneration of spent LiFePO4 by direct chemical lithiation

Tassadit Ouaneche, Matthieu Courty, Lorenzo Stievano, Laure Monconduit, Claude Guéry, Moulay T Sougrati, Nadir Recham

Room temperature efficient regeneration of spent $LiFePO_4$ by direct chemical lithiation

Tassadit Ouaneche[1,2,3], Matthieu Courty[1,3], Lorenzo Stievano[2,3,4], Laure Monconduit[2,3,4], Claude Guéry[1,3,4], Moulay T. Sougrati[2,3,4*] and Nadir Recham[1,3,4*]

[1] Laboratoire de Réactivité et de Chimie des Solides (LRCS), CNRS UMR 7314, Université de Picardie Jules Verne, 80039 Amiens, Cedex 1, France

[2] ICGM, Univ. Montpellier, CNRS, ENSCM, 34090 Montpellier, France

[3] Réseau Français sur le Stockage Electrochimique de l'Energie (RS2E), FR CNRS 3459, F-80039 Amiens, Cedex 1, France

[4]ALISTORE-ERI European Research Institute, FR CNRS 3104, Amiens F-80039 Cedex 1, France

Abstract:

With the exponential production of lithium-ion batteries for electric and electronic applications, there is an urgent need for efficient recycling of spent batteries in order to mitigate environmental pollution and limit the waste of valuable and critical resources. Herein, we report a rewarding direct recycling process of the $LiFePO_4$ cathode material by direct room temperature chemical lithiation (DCL) in solution. In the case of liquid organic electrolytes, a fine characterization of a recovered LFP cathode from a spent commercial battery demonstrates that the end of life of the battery is mainly due to the lithium loss, while the structure of the LFP cathode material is globally preserved. It is shown here that such a cathode can be efficiently recovered by direct lithiation in solution using LiI in different solvents (acetonitrile, ethanol, cyclohexane, methanol, DMSO and propan-1,2-ol) with optimized experimental parameters. The best electrochemical performance is obtained with ethanol, one of the greenest and cheapest solvents, without any additional heat treatment. More interestingly, the regeneration of LFP can be achieved directly with the material casted onto its aluminum collector, which paves the way to more efficient recycling preserving the whole electrode formulation and avoiding a new electrode casting. The chemically lithiated LFP cathode in ethanol exhibits a full reversible

capacity of ~168 mAh/g *vs*. Li metal with a stable coulombic efficiency exceeding 98% for 25 cycles. In addition, this recovery process produces regenerated electrodes showing good electrochemical performance also at high current density.

* Corresponding authors: nadir.recham@u-picardie.fr
moulay-tahar.sougrati@umontpellier.fr

Keywords: Direct recycling**,** Lithium ion battery, $LiFePO_4$, chemical lithiation, regeneration.

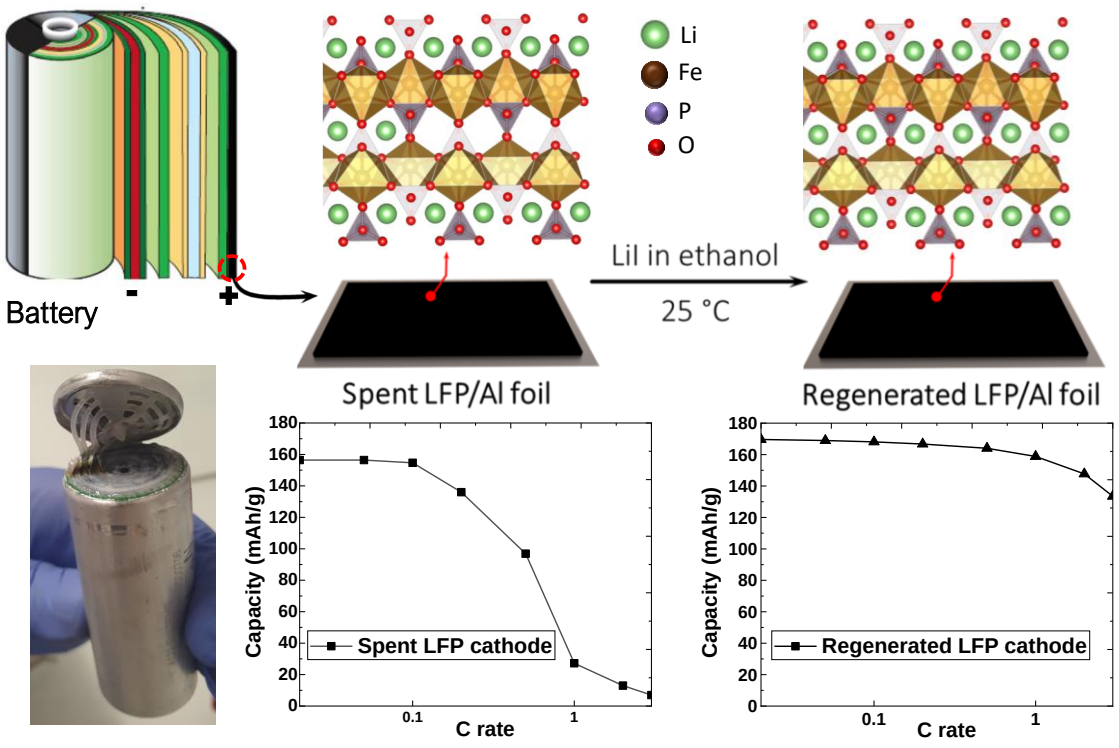

Introduction

Nowadays, in front of the global climate change and the large use of energy, there is a huge increasing shortage of global resources all over the world. This involves a real need for environmental protection by considerably reducing both natural resources consumption and environmental pollution[1,2].

Over the past few decades, there has been a great interest in lithium-ion batteries (LIBs) which have been widely used for many applications, ranging from portable electronics to electric vehicles (EV)[3]. The advantages of LIBs application in EV are energy density, long cycle life, low CO_2 emission[4]. However, an electric vehicle battery is considered at the end-of-life when its capacity goes below 80% of the pristine one, presaging a large stock of spent batteries in the next years[5] adding to the already existing stock of portable electronics batteries. It is noteworthy that used EV batteries could have a second use, such batteries could still perform sufficiently to serve in less-demanding applications, such as stationary energy-storage services.

Repairing a spent electrode without the need of heavy chemical processes remains however the holy grail. The use of lithium iron phosphate, $LiFePO_4$, as positive electrode in LIBs is nowadays increasing and is expected to become one of the most widely commercially used cathodes because of its safety[6], low cost, thermal stability, reliability and long cycle life[7]. Its application is expected to rise, in particular, in the rapidly growing industry of electric vehicles, which will replace thermic vehicles in the coming years[8]. In the US, for instance, several states have planned to move to 100% zero-emission vehicles by 2050[3]. In China, around 313 300 tons of spent LFP batteries will likely need to be recycled by 2030[5]. In addition, the new EU standards for ethical and more sustainable batteries foresees an increased implementation of their recycling as a necessary action to limit their carbon footprint. To reach this goal, 70% of portable batteries must be collected for recycling by 2025. From 2030, industrial and electric vehicle batteries will have to meet minimum recycled content requirements (12% cobalt, 85% lead, 4% lithium and 4% nickel)[9].

The industrial recycling methods currently used for LIBs are (i) pyrometallurgy, a thermal metallurgical process based on high temperature heating under controlled atmosphere to recover metals and/or alloys, and (ii) hydrometallurgy, which requires a complete or selective dissolution of cathode materials followed by precipitation steps to recover mostly metal salts. These methods require multiple steps, high energy and large amounts of chemicals. Moreover,

after the destructive treatments applied by these two recycling processes, not only a substantial part of cathodes' value is lost but a huge chemical waste is produced. Hence, there is a real need to considerably reduce the waste production and energy cost especially for cathode materials that do not contain critical and/or expensive metals, (*e.g.*, Co and Ni), such as $LiFePO_4$. This is due to the economic value of its recycled products, which is lower than that of its recovery via costly pyrometallurgical and hydrometallurgical processes[10,11]. In addition, when pyrometallurgy is used, lithium can be lost by volatilization due to its low atomic mass[12].

Hence, there is an urgent need to develop ecological recycling processes to reduce the environmental impact of LFP-based LIBs and face possible future shortage of some of their components (*e.g.*, lithium)[13]. To achieve this, direct recycling is considered as the most adapted method to regenerate LFP electrodes. This approach does not require going through destruction steps in solution or at high temperature, it seeks to minimize energy consumption and cost while preserving the environment via a rational use of resources, materials and energy[14,15].

Several studies on the aging of $LiFePO_4$ revealed that the major reasons for the end of life of LFP batteries are either the irreversible loss of lithium[10], consumed by parasite reactions such as the growth of the Solid Electrolyte Interphase (SEI) during cycling[16,17], by a deterioration of the carbon coating or by a structural defect caused by the partial migration of Fe^{2+} from the M2 site into the M1 site of LFP, usually occupied by Li^+, which causes anti-sites defects and blocks Li^+ diffusion in the structure along the b-axis[18,19].

In the literature, few processes are reported for the direct recycling of LFP cathodes[20]. The three major ones are i) thermal treatment after adding a lithium source, ii) electrochemical lithiation and iii) chemical lithiation. Chen *et al.* proposed a carbothermal reduction method to prepare $LiFePO_4$ from Li_2CO_3 and olivine $FePO_4$ recovered from spent LFP cathodes via oxidizing leaching[5,21]. The regenerated $LiFePO_4$ shows an initial discharge specific capacity of 146.89 mAh/g *vs.* Li^+/Li^0 at 1C. Electrochemical lithiation via pre-lithiated graphite was suggested as an alternative by Wang *et al*. In this case, the specific capacity of the full cell with spent LFP and pre-lithiated graphite is 90.4 mAh/g in charge, while 126.6 mAh/g are recovered in the following discharge[22]. In addition, based on the reducing power of lithium iodide (LiI) reported by Popov *et al.*[23], its ability to reduce $FePO_4$ to $LiFePO_4$ was used by *Laffont et al.*[24] to chemically lithiate spent LFP cathodes by immersing them in LiI/acetonitrile solutions. Ganter *et al.* similarly reported an electrochemical and chemical lithiation method of spent LFP

cathodes, which led regaining a capacity of 150-155 mAh/g[25]. Recently, Gangaja *et al.* showed a facile way to regenerate spent LFP electrode using LiI in acetonitrile, showing a discharge capacity of 150 mAh/g at 1C for the regenerated LFP[26].

Herein, our purpose is to put forward a new green direct recycling process of spent LFP cathodes after their full characterization in terms of structure, morphology and electrochemical properties. In particular, it will be shown how the properties of the LFP cathode regenerated by direct chemical lithiation in LiI solutions depends on the solvent as well as the regeneration temperature.

Experimental section

LFP recovery from spent batteries

The spent $LiFePO_4$ (LFP) cathode material was recovered from a cycled 2.3 Ah commercial cell type A123 Systems (LFP/graphite 26650 cylindrical cell). This battery, produced in 2009-2010, was aged in the laboratory during another project, and stored for ~10 years in a refrigerator at 5 °C before being recovered for this study.

After a preliminary evaluation of its charge state, the cell was then opened following a safe experimental protocol, by first discharging it to 0.5 V, and then disassembling it carefully in a dry room using a pipe cutter and a micro flush cutter to remove the can. The battery was not discharged to a lower potential in order to prevent the copper current collector oxidation at the negative electrode which might lead to copper shuttling in the electrolyte and subsequently cathode pollution. After unrolling the electrodes and separating them from the separator, the positive electrode was recovered, carefully washed in dimethyl carbonate DMC and dried under primary vacuum at 90 °C. The cathode material was then used either as a powder, by scraping it from the aluminum current collector, or directly as an electrode by punching out 13 mm diameter discs from the original electrode stripe.

Regeneration process

For the regeneration of the LFP-based cathode material including both polymer binder and conductive carbon additive, 1 g of the cathode powder removed from the current collector was first immersed in 50 ml of acetonitrile (HiPerSolv Chromanorm, 99.9%). Then, 266.4 mg of lithium iodide LiI (Acros Organics, 99%), corresponding to a molar ratio LiI/FP of 1 for a FP content of 30% in the cathode powder, demonstrated by Mössbauer spectroscopy and

electrochemistry below, were added to the suspension. The powder was recovered by filtration with a 0.1 µm polypropylene filter and washed several times with acetonitrile to remove all the remaining iodine species. The sample was then dried under primary vacuum at 100 °C for 1 hour, and finally ground to fine powder in a mortar.

A similar process was performed also using other solvents at the place of acetonitrile, such as ethanol (Sigma-Aldrich, purity 95.6%), cyclohexane (Sigma-Aldrich, purity 99.5%), methanol (VWR, purity 99.9%), dimethylsulfoxyde DMSO (VWR, purity 99.9%) and propan-1,2-ol (Sigma-Aldrich, purity 99.5 %). These solvents were chosen based on their low price, their green and non-toxic nature and their potential ability to allow the total regeneration of the spent LFP in the best conditions while consuming minimum energy. Among these solvents, ethanol is the greenest and the cheapest one[33].

Finally, we show here for the first time that LFP can be repaired without the need of the Al collector removal. This paves the way to simplified regeneration processes provided that some corrosion issues are solved.

Reference $FePO_4$ preparation

Pure $FePO_4$ powder, used to highlight the possible chemical reduction of $FePO_4$ into $LiFePO_4$ accompanied by lithium insertion in the structure was prepared by chemical delithiation of commercial $LiFePO_4$ by soluble Fe^{3+} in water. Typically, 15 g of commercial $LiFePO_4$ were dispersed in 100 ml of water, then 40 g of $Fe(NO_3)_3.9H_2O$ were added to the solution, which was stirred at room temperature under ambient air for 10 hours. The recovered $FePO_4$ powder was filtered, washed with distilled water and acetone, and finally dried in air in an oven at 70 °C.

Characterization techniques

Crystallographic analysis was carried out using a Bruker D8 Advanced X-ray Diffractometer with Cu K_α radiation ($\lambda K_{\alpha1}$= 1,54056 Å and $\lambda K_{\alpha2}$= 1,54439 Å) operating in reflection mode in the range 2θ = 10-70° with a 2θ step size of 0.085°. The obtained X-ray diffraction (XRD) patterns were refined using full pattern matching via the Fullprof software in order to obtain the lattice parameters. Particle morphology and chemical composition were characterized by Scanning Electron Microscopy (SEM, FEI Quanta 200-FEG) coupled with Energy Dispersive X-ray Spectroscopy (EDX).

For iron speciation, transmission ^{57}Fe Mössbauer spectra were measured in the constant acceleration mode with a ^{57}Co:Rh source. The spectrometer was calibrated at 295 K with an α-iron foil. The absorbers used in this work contained 20-50 mg/cm^2 of LFP/PVDF/C powder or film.

Thermogravimetric analysis (TGA) experiments were performed in air flow, using a STA 449C Jupiter unit type device (Netzsch Inc.) coupled with DSC Differential Scanning Calorimetry and mass spectrometry, in order to evaluate the thermal stability of the constituents as well as the weight ratio of active material in the spent electrode. The powders were heated from ambient temperature up to 900 °C, with a heating rate of 10 °C/min.

Fourier Transform-Infrared (FTIR) spectra were recorded through a Nicolet iS20 spectrometer. The powders were analysed in the ATR (Attenuated Total Reflection) mode to determine the nature of the polymer binder contained in the spent cathode. Since in our case no trace of fluorine-containing products could be detected by TGA, FTIR spectroscopy was used to identify the nature of the polymer binder. In order to enhance the possible signal of the PVDF binder, a measurement of a mixture of commercial pristine LFP with carbon was used as the spectral background.

The electrochemical characterization of the spent LFP-based commercial battery was carried out by cycling it in the galvanostatic mode with a multichannel battery tester (SBT2050, PEC, Belgium) at 25°C between 2.1 and 4.2 V. After aging, the cell was discharged to 0.5 V before being disassembled. The electrochemical properties of the electrodes at different stages of the regeneration process were studied in half-cell configuration *vs.* Li metal foil in Swagelok™-type cells assembled in an argon-filled glove box using 10 mg of electrode composite powder (carbon/LFP mixture) or directly using the regenerated electrode supported on its original current collector. The two electrodes were separated by two sheets of glass fibre disks soaked with a 1M solution of $LiPF_6$ in an ethylene carbonate (EC)/dimethyl carbonate (DMC) mixture (1/1 w/w).

Results and discussion

Characterisation of the spent cathode

Before opening, the state of the spent LFP-based battery was checked by performing some galvanostatic cycles (**Fig. 1a**), which showed (i) that the battery is still able to cycle, and (ii) that it follows the typical electrochemical profile of a conventional LFP/Graphite battery.

However, a reversible capacity of only 105 mAh/g (1.38 Ah) is observed, which corresponds to 60% of the theoretical capacity of the LFP. It indicates that this battery is beyond the expected end of life (EOL) limits, especially for an EV application. As mentioned in the introduction, the failure or the decrease of the performance of an LFP LIB is generally attributed to three possible reasons: i) irreversible lithium trapping, ii) structural defect and iii) carbon coating degradation. To determine the reason(s) of the end of life (EOL) of this battery, a *post mortem* diagnosis was performed on the positive electrode recovered after unrolling the electrodes and separating them from the separator (**Fig. 1b**).

The refinement of the XRD pattern of the LFP cathode in the discharged state shown in **Fig. 2a** indicates the presence of two olivine phases, triphylite $LiFePO_4$ (space group Pnma, a = 10.317(1) Å, b = 5.996(1) Å, c = 4.702(1) Å and V = 290.83(2) Å^3) and a significant amount of heterosite $FePO_4$ (space group Pnma, a = 9.851(1) Å, b = 5.810(1) Å, c = 4.772(1) Å and V = 273.12(2) Å^3), which evidences a substantial lithium deficiency in the cathode material. The refined cell parameters of both phases are in good agreement with literature reports[27,28].

The lithium deficiency is confirmed by Mössbauer spectroscopy (**Fig. 2b**, and corresponding fitting parameters in **Table 1**), which indicates the presence of 65% Fe^{II} ($LiFePO_4$) and 19% Fe^{III} ($FePO_4$). It is worth noting that the observation of only one Fe^{2+} environment rules out the presence of any structural defect such as the anti-sites ones, in the structure[19]. Two other Fe^{III} environments are detected (8.3% and 7.7%) and can be attributed either to some amorphous impurities probably present in fresh electrode, such as Fe_2P or Fe_3P which are known to form during the synthesis of the pristine material at high temperatures in a reductive environment[29]. Similar impurities have been identified in new LFP cells.

The electrode material recovered from the spent electrode was analysed by TGA-MS under air to determine its content in active material (including both LFP and FP). The TGA-MS results (**Fig. 3a**) show different mass losses: at temperatures lower than 200 °C, a first mass loss of about 1% is observed, which corresponds to the desorption of water physisorbed on the powder surface, while an additional mass loss of about 4% is observed between 200 and 350 °C, which corresponds to the emission of H_2O/CO_2. This second process is probably due to the decomposition of the polymer binder. Finally, a mass loss of 6% in three consecutive steps corresponding to the emission of CO_2 is observed between 350-900 °C, which can be attributed to the oxidation of the carbon contained in the cathode material (including both conductive carbon and coating carbon).

Considering that during the TGA measurement in air, some of the pristine LFP is converted at high temperatures to Fe_2O_3 according to equation (1)[30]:

$$3\ LiFePO_4 + ¾\ O_2 \rightarrow Li_3Fe_2(PO_4)_3 + ½\ Fe_2O_3 \ldots (1)$$

this quantitative evaluation demonstrates that this cathode contains ~85% active material. The formation of Fe_2O_3 could be confirmed by XRD analysis of the sample recovered from the TGA measurement (**Fig. S1**). In the FTIR spectrum of the spent electrode material, shown in **Fig. 3b**, the absorption peaks at 1168 and 1275 cm^{-1} indicate the presence of CF_2 groups while the band at 1402 cm^{-1} identifies CH_2 group confirming the presence of PVDF as the polymer binder in this electrode.

The electrochemical performance (**Fig. 4a**) of spent LFP was evaluated in half cell *vs.* lithium metal at a current rate of C/10 (reaction of one mole of lithium per mole of LFP in 10 hours). The charge-discharge curve exhibits the typical signature of LFP with a flat plateau centred at 3.44 V. The first discharge is only partial, and corresponds to the reduction of the fraction of $FePO_4$ remaining in the sample to $LiFePO_4$ after discharge to 0.5 V. This means that this amount of active Fe^{III} corresponds to the amount of missing lithium in the electrode (about 30%), in full agreement with the XRD and Mössbauer spectroscopy results.

The first charge reaches a capacity of ~ 161.5 mAh/g, which corresponds to 95% of the theoretical capacity of LFP. This improvement demonstrates the ability to regenerate this type of cathodes by electrochemical lithiation in half cells *vs.* Li metal, as previously demonstrated by Ganter *et al*., even though the possible scale-up of such a process remains delicate[25]. A study of the rate capability of this sample (**Fig. 4b)** registered between C/100 and 3C, on the other hand, indicates a poor electrochemical performance at high C-rates: the material loses the total capacity already at a current rate of 1C probably due to lower electrode conductivity linked to the lithium trapping in the growing SEI.

In conclusion, the characterisation of the spent LFP cathode studied here shows that its observed capacity loss (30%) is due to irreversible lithium trapping in the battery, and that the full capacity can be recovered by electrochemical lithiation. It is therefore possible, in principle, to regenerate the cathode by direct chemical lithiation.

Regeneration process

The spent LFP cathode powder recovered after regeneration in a LiI acetonitrile solution was characterised by XRD (**Fig. 5a**), which shows that the $FePO_4$ phase has completely

disappeared and that the only crystalline phase contained in the sample is $LiFePO_4$ (lattice parameters $a = 10.313(1)$ Å, $b = 5.994(1)$ Å, $c = 4.703(1)$ Å and $V = 290.69(1)$ Å^3). This confirms that the Fe^{III} is completely reduced to Fe^{II}, and that this reduction is accompanied by lithium insertion in the $FePO_4$ structure, following reaction (2):

$$FePO_4 + LiI \xrightarrow{\text{Acetonitrile}} LiFePO_4 + \tfrac{1}{2} I_2 \ldots (2)$$

The comparison of the morphology of the spent LFP-containing cathode material with that of the same material after chemical lithiation (**Fig. 5b** and **5c,** respectively) does not show any significant difference between the two samples, implying that particles morphology is preserved.

To check the efficiency of this lithiation process in the case of electrodes containing larger portions of $FePO_4$, the same process was applied directly to pure FP confirmed by XRD and Moss spectroscopy (Fig 6). The chemical reaction of this $FePO_4$ powder in LiI acetonitrile solution results, also in this case, in its complete reduction lithiation according to reaction (2), as testified by XRD (**Fig. 6a**).

It is interesting to notice that the I_2/I^- couple can be used both for $FePO_4$ reduction into $LiFePO_4$ using I^- in acetonitrile solutions[25], as well as for $LiFePO_4$ delithiation into $FePO_4$ using I_2 aqueous solutions[31]. In order to better understand this ambiguous behaviour, and to take into account the relatively complex properties of the I_2/I^- and I_3^-/I^- redox couples[32], the equilibrium potentials of the I_2/I^- redox couple were first measured in water, acetonitrile and other few solvents with physicochemical properties close to those of water or acetonitrile at room temperature, including ethanol, cyclohexane, methanol, DMSO and propan-1,2-ol. The measurement of the potential of different solutions of 0.5 M LiI in these solvents, performed in a two-electrode electrochemical cell with saturated calomel electrode (SCE) as reference, and a platinum wire as the working electrode are reported in **Table 2**. Regarding the FP/LFP redox couple potential of 0.44 V *vs*. NHE, cyclohexane and acetonitrile (highest potential difference) are expected to be the most favourable solvents for FP reduction.

The possible direct lithiation of the spent LFP using the alternative solvents mentioned above was therefore investigated under the same conditions as with acetonitrile in terms of $LiI/FePO_4$ ratio (summary is in **Table 3**), but by adjusting some parameters such as temperature and reaction time. In the case of ethanol, for instance, the reaction time was extended to 48 h. For methanol, the Li^+ concentration was increased by adding another soluble lithium source as

lithium acetylacetonate (Aldrich, purity 97%), to promote the reaction and destabilize the solvation sphere. This can be explained by the availability of lithium in the solution, as it is very solvated and stable in the solution, so it is imperative to destabilize the solvation sphere and promote the lithium diffusion into the structure to get the full lithiation of the LFP phase. In DMSO, both lithium concentration and temperature were adjusted, lithium acetylacetonate was added to increase Li^+ concentration and the solution was heated at 70 °C for 24 h to accelerate the reaction kinetics. This reaction could also be carried out at room temperature, but with longer reaction times (about 4 days). It is worth noting that a fine optimisation of all parameters affecting the FP lithiation kinetics is not in the scope of this paper.

With the exception of water, the redox potentials solutions prepared starting from LiI and containing traces of I_2, measured for the different solvents and/or the corresponding standard potentials of the I_2/I^- couple reported in the literature agree with the spontaneous reduction and relithiation of FP in the proposed LiI solutions. Indeed, in all the reported conditions, a total regeneration of the spent LFP cathode is observed (**Fig. 7**), which shows the presence of pure LFP for all the regenerated cathode materials. These results are confirmed in the cases of acetonitrile and ethanol by Mössbauer spectroscopy (**Fig. 8a** and **8b**, respectively), which shows the presence of the typical symmetric doublet of octahedral high spin Fe^{2+} in $LiFePO_4$ with an isomer shift of 1.22 mm/s and a quadrupole splitting of 2.95 mm/s. In all the spectra, a minor doublet is observed with parameters close to those of the impurities already contained in pristine fresh electrodes recovered from new LFP cells (different batch). Finally, the preservation of the conductive carbon amount was confirmed by thermogravimetric analysis under air which indicated the same carbon weight ratio as before regeneration (**Fig. S2**).

The LFP powders regenerated in different solvents were first electrochemically evaluated versus Li^+/Li^0. Without the addition of any conductive carbon additive, the material exhibits very poor electrochemical performance in terms of specific capacity and polarization as shown in **Fig. 9a**. By adding 10 wt.% conductive carbon, however, the material shows the typical electrochemical LFP signature and better electrochemical properties with a reversible capacity of about ~130 mAh/g (**Fig. 9b**) and an average potential of 3.44 V. The bad performance observed in the absence of carbon additive could be due to the unsuited formulation for these regenerated electrode powders.

To address this cyclability issue, the same regeneration process was tested directly with complete electrode pieces of 3 × 3 cm cut from the spent LFP cathode without peeling out the active material from the aluminum current collector.

The first cycle curves for the regenerated LFP electrode disks in acetonitrile and ethanol (the two best solvent) used as positive electrode versus Li^+/Li^0 at a current rate of C/10 (**Fig. 10a** and **10c**, respectively) show the typical signature of LFP and an average potential of 3.44 V. For both materials, a very low discharge capacity is obtained (< 2%), which indicates the total relithiation of FP during the regeneration, in agreement with XRD and Mössbauer spectroscopy results. Both regenerated materials exhibit a reversible capacity of ~168 mAh/g in the following charge and discharge processes. In the case of acetonitrile however (**Fig. 10b**), the coulombic efficiency is unstable, and decreasing to 93% at the 25^{th} cycle. In the case of ethanol, the electrode exhibits a good reversibility for 25 cycles and low polarization, with a higher coulombic efficiency exceeding 98% (**Fig. 10d**).

The rate capability between C/50 and 3C of the LFP electrodes regenerated in acetonitrile and ethanol is shown in **Fig. 11a** and **11b** during the charges and the discharges respectively, and compared to the performance of the spent LFP electrode before regeneration. For the charge, the LFP electrode chemically lithiated in the LiI acetonitrile solution exhibits a capacity of 150 mAh/g at 1C, while a capacity of 161 mAh/g is observed for the sample regenerated in LiI ethanol solution. In discharge, the capacity of the chemically lithiated LFP electrode is about 144 and 160 mAh/g in acetonitrile and ethanol, respectively, at 1C. These results show that the best performance is obtained for the LFP regenerated in LiI ethanol solution, and that such a cathode is still suitable for high power applications. It's worth mentioning that, after the LiI treatment, the Al current collector shows minor traces of corrosion (**Fig. S3**), and that further work is needed to suppress this side effect. Finally, one should notice a substantial improvement of the rate capability performance of the regenerated LFP electrodes compared to spent electrodes. This improvement could also depend on the possible removal of the solid electrolyte interphase SEI from the spent cathode electrode during the regeneration in solution.

Conclusions

Spent LFP cathodes, which lost part of their capacity and rate capability during long term cycling in LIBs because of irreversible lithium trapping and SEI, could successfully recover their pristine performance with the application of a rewarding direct chemical lithiation process using LiI dissolved in different solvents (acetonitrile, ethanol, cyclohexane, methanol, DMSO and propan-1,2-ol) after optimisation of different parameters such as temperature, lithium amount and time reaction. The regeneration could be carried out also on complete LFP cathodes supported on their original current collectors, in spite of some minor corrosion of the Al collector by I_2.

The proposed LFP cathode regeneration method preserves electrode formulation and carbon coating and therefore paves the way to a more sustainable LFP-based LiBs recycling, since it can be carried out using a green solvent such as ethanol, and in the absence of any additional heat treatment, which will certainly be useful for recycling the large stock of spent LFP batteries in the next years.

Acknowledgement

The authors gratefully acknowledge the RS2E for the funding of this thesis, Prof. P. Barboux and Dr A. Mohammadi for the fruitful discussions. We also thank C. Delacourt for providing us the LFP commercial batteries used for this work.

References

1. Neumann, J. *et al.* Recycling of Lithium-Ion Batteries—Current State of the Art, Circular Economy, and Next Generation Recycling. *Adv. Energy Mater.* **12**, 2102917 (2022).

2. Armand, M. & Tarascon, J.-M. Building better batteries. *Nature* **451**, 652–657 (2008).

3. Muratori, M. *et al.* The rise of electric vehicles—2020 status and future expectations. *Prog. Energy* **3**, 022002 (2021).

4. Tarascon, J.-M. *et al.* Hunting for Better Li-Based Electrode Materials via Low Temperature Inorganic Synthesis. *Chem. Mater.* **22**, 724–739 (2010).

5. Chen, B. *et al.* Regeneration and performance of LiFePO4 with Li_2CO_3 and $FePO_4$ as raw materials recovered from spent $LiFePO_4$ batteries. *Mater. Chem. Phys.* **279**, 125750 (2022).

6. Perea, A. *et al.* State of charge influence on thermal reactions and abuse tests in commercial lithium-ion cells. *J. Power Sources* **399**, 392–397 (2018).

7. Zaghib, K., Mauger, A., Goodenough, J. B., Gendron, F. & Julien, C. M. Electronic, Optical, and Magnetic Properties of LiFePO 4 : Small Magnetic Polaron Effects. *Chem. Mater.* **19**, 3740–3747 (2007).

8. Wang, M. *et al.* Recycling of lithium iron phosphate batteries: Status, technologies, challenges, and prospects. *Renew. Sustain. Energy Rev.* **163**, 112515 (2022).

9. European Parliament. *EU Legislation in Progress New EU regulatory framework for batteries Setting sustainability requirements*. (2022).

10. Xu, P. *et al.* Efficient Direct Recycling of Lithium-Ion Battery Cathodes by Targeted Healing. *Joule* **4**, 2609–2626 (2020).

11. Latini, D. *et al.* A comprehensive review and classification of unit operations with assessment of outputs quality in lithium-ion battery recycling. *J. Power Sources* **546**, 231979 (2022).

12. Chen, M. *et al.* Recycling End-of-Life Electric Vehicle Lithium-Ion Batteries. *Joule* **3**, 2622–2646 (2019).

13. Steward, D., Mayyas, A. & Mann, M. Economics and Challenges of Li-Ion Battery

Recycling from End-of-Life Vehicles. *Procedia Manuf.* **33**, 272–279 (2019).

14. Jin, Y., Zhang, T. & Zhang, M. Advances in Intelligent Regeneration of Cathode Materials for Sustainable Lithium-Ion Batteries. *Adv. Energy Mater.* **12**, 2201526 (2022).

15. Larcher, D. & Tarascon, J.-M. Towards greener and more sustainable batteries for electrical energy storage. *Nat. Chem.* **7**, 19–29 (2015).

16. Palacín, M. R. & de Guibert, A. Why do batteries fail? *Science (80-.).* **351**, (2016).

17. Zhou, S. *et al.* Direct recovery of scrapped $LiFePO_4$ by a green and low-cost electrochemical re-lithiation method. *Green Chem.* **24**, 6278–6286 (2022).

18. Safari, M. & Delacourt, C. Aging of a Commercial Graphite/LiFePO4 Cell. *J. Electrochem. Soc.* **158**, A1123 (2011).

19. Padhi, A. K., Nanjundaswamy, K. S., Masquelier, C., Okada, S. & Goodenough, J. B. Effect of Structure on the Fe^{3+} / Fe^{2+} Redox Couple in Iron Phosphates. *J. Electrochem. Soc.* **144**, 1609–1613 (1997).

20. Kumar, J. *et al.* Recent progress in sustainable recycling of $LiFePO_4$-type lithium-ion batteries: Strategies for highly selective lithium recovery. *Chem. Eng. J.* **431**, 133993 (2022).

21. Zhang, J. *et al.* Sustainable and Facile Method for the Selective Recovery of Lithium from Cathode Scrap of Spent LiFePO 4 Batteries. *ACS Sustain. Chem. Eng.* **7**, 5626–5631 (2019).

22. Wang, T. *et al.* Direct regeneration of spent $LiFePO_4$ via a graphite prelithiation strategy. *Chem. Commun.* **56**, 245–248 (2020).

23. Popov, A. I. & Geske, D. H. Studies on the Chemistry of Halogen and of Polyhalides. XIII. Voltammetry of Iodine Species in Acetonitrile. *J. Am. Chem. Soc.* **80**, 1340–1352 (1958).

24. Laffont, L. *et al.* Study of the $LiFePO_4$ /$FePO_4$ Two-Phase System by High-Resolution Electron Energy Loss Spectroscopy. *Chem. Mater.* **18**, 5520–5529 (2006).

25. Ganter, M. J., Landi, B. J., Babbitt, C. W., Anctil, A. & Gaustad, G. Cathode

refunctionalization as a lithium ion battery recycling alternative. *J. Power Sources* **256**, 274–280 (2014).

26. Gangaja, B., Nair, S. & Santhanagopalan, D. Reuse, Recycle, and Regeneration of LiFePO 4 Cathode from Spent Lithium-Ion Batteries for Rechargeable Lithium- and Sodium-Ion Batteries. *ACS Sustain. Chem. Eng.* **9**, 4711–4721 (2021).

27. Padhi, A. K., Nanjundaswamy, K. S. & Goodenough, J. B. Phospho-olivines as Positive-Electrode Materials for Rechargeable Lithium Batteries. *J. Electrochem. Soc.* **144**, 1188–1194 (1997).

28. Recham, N., Armand, M., Laffont, L. & Tarascon, J.-M. Eco-Efficient Synthesis of LiFePO[sub 4] with Different Morphologies for Li-Ion Batteries. *Electrochem. Solid-State Lett.* **12**, A39 (2009).

29. Konarova, M. & Taniguchi, I. Physical and electrochemical properties of $LiFePO_4$ nanoparticles synthesized by a combination of spray pyrolysis with wet ball-milling . *J. Power Sources* **194**, 1029–1035 (2009).

30. Morcrette, M., Wurm, C. & Masquelier, C. On the way to the optimization of $Li_3Fe_2(PO_4)_3$ positive electrode materials. *Solid State Sci.* **4**, 239–246 (2002).

31. Steen, I. *et al.* (12) United States Patent (10) Patent No .: vol. 2 (2014).

32. Huang, Q., Yang, J., Ng, C. B., Jia, C. & Wang, Q. A redox flow lithium battery based on the redox targeting reactions between $LiFePO_4$ and iodide. *Energy Environ. Sci.* **9**, 917–921 (2016).

33. Byrne, F. P. *et al.* Tools and techniques for solvent selection: green solvent selection guides. *Sustain. Chem. Process.* **4**, 7 (2016).

34. Boschloo, G. & Hagfeldt, A. Characteristics of the Iodide/Triiodide Redox Mediator in Dye-Sensitized Solar Cells. *Acc. Chem. Res.* **42**, 1819–1826 (2009).

35. Takahashi, K., Shibagaki, M., Kuno, H., Kawakami, H. & Matsushita, H. The Amidation of Carboxylic Acid with Amine over Hydrous Zirconium(IV) Oxide. *Bull. Chem. Soc. Japan* **62**, 1333–1334 (1989).

36. Bentley, C. L., Bond, A. M., Hollenkamp, A. F., Mahon, P. J. & Zhang, J. Voltammetric Determination of the Iodide/Iodine Formal Potential and Triiodide Stability Constant in

Figure Captions

Fig. 1: a) Voltage-composition curve of LFP/graphite battery before opening and **b)** images showing the two electrodes, LFP cathode on its aluminum current collector and anode on a copper current collector, recovered after opening the battery in a dry room.

Fig. 2: a) X-ray diffraction pattern refinement and **b)** Mössbauer spectra of spent $LiFePO_4$ powder cathode material.

Fig. 3: a) Thermogravimetric analysis coupled with TGA-MS made under air between room temperature and 900 °C with a heating rate of 10 °C / min and **b)** Infrared spectra registered in ATR mode for the spent $LiFePO_4$ powder cathode material.

Fig. 4: a) Charge-discharge galvanostatic curves at C/10 (1 electron in 10 hours) of the spent LFP cathode as positive electrode *vs*. Li^+/Li^0, its derivative curve and **b)** the high-power cycling for the different rates between C/100 and 3C of the spent LFP cathode.

Fig. 5: a) XRD patterns of 1) spent LFP cathode material before regeneration and 2) after regeneration in acetonitrile and Scanning electron microscopy (SEM) images of **b)** spent LFP cathode and **c)** chemically lithiated LFP cathode in acetonitrile.

Fig. 6: a) XRD patterns of **1)** pristine commercial LFP powder, **2)** chemically delithiated commercial FP phase and **3)** lithiated LFP in acetonitrile, **b)** Mössbauer spectra of the chemically delithiated FP phase.

Fig. 7: XRD patterns of **a)** spent LFP cathode powder material followed by the regenerated LFP cathode using LiI in **b)** ethanol, **c)** cyclohexane, **d)** methanol, **e)** DMSO and **f)** propan-1,2-ol.

Fig. 8: Mössbauer spectra of regenerated LFP cathode in **a)** acetonitrile and in **b)** ethanol.

Fig. 9: Charge/discharge galvanostatic curve at C/10 for Li half-cell using **a)** the regenerated LFP powder in acetonitrile and **b)** the regenerated LFP powder in acetonitrile with 10 wt.% carbon as the positive electrode with its inserted derivative curve.

Fig. 10: Charge/discharge galvanostatic curves at C/10 for Li half-cells, using the regenerated LFP electrode disks in **a)** acetonitrile with **b)** its cyclability and coulombic efficiency and the

regenerated LFP electrode disks in **c)** ethanol as the positive electrode and their respective derivative curves with **d)** its cyclability and coulombic efficiency.

Fig. 11: The high-power cycling **a)** charge and **b)** discharge at different rates between C/50 and 3C using the regenerated LFP cathode disks in acetonitrile and in ethanol as the positive electrode *vs*. Li^+/Li^0.

Tables

Table 1: Fitted Mössbauer parameters of typical spent and regenerated LFP. IS, QS, LW and Abs are respectively the isomer shift, the quadrupole splitting, the linewidth and the relative absorption areas

Samples	IS, mm/s	QS, mm/s	LW, mm/s	Abs, %	Attribution
Spent LFP	1.22	2.96	0.26	65.2	LFP (Fe^{2+})
	0.42	1.56	0.26	16.8	FP (Fe^{3+})
	0.50	1.19	0.35	9.5	(Fe^{3+})
	0.47	0.77	0.35	8.5	(Fe^{3+})
Delithiated FP	0.41	1.52	0.25	100	FP (Fe^{3+})
Regenerated LFP in acetonitrile	1.22	2.95	0.26	93.4	LFP (Fe^{2+})
	0.45	0.76	0.35	6.3	(Fe^{3+})
Regenerated LFP in ethanol	1.22	2.95	0.29	89	LFP (Fe^{2+})
	0.45	0.75	0.60	11	(Fe^{3+})

Table 2: Measured equilibrium potentials (V/NHE) of different solutions containing I^-

	Solvents						
	Water	Acetonitrile	Ethanol	Cyclohexane	Methanol	DMSO	Propan-1,2-ol
Equilibrium potentials (V/NHE)	0.538	0.268	0.418	0.258	0.305	0.310	0.362
Standard potential I_2/I^-	0.536[34]	0.217[35]	0.196[36]	-	-	-	-

Table 3: Optimization of the regeneration process conditions according to the used solvent

Solvents	**Acetonitrile**	**Cyclohexane**	**Ethanol**	**Methanol**	**DMSO**	**Propan-1,2-ol**
T °C	Ambient	Ambient	Ambient	Ambient	70	Ambient
Li source	LiI	LiI	LiI	LiI/LiAcAc	LiI/LiAcAc	LiI
Time	20 h	24 h	48 h	24 h	24 h	24 h
Origin	VWR	Sigma-Aldrich	Sigma-Aldrich	VWR	VWR	Sigma-Aldrich
Purity	99.95 %	99.5 %	95.6 %	99.9 %	99.9 %	99.5 %

Figures.

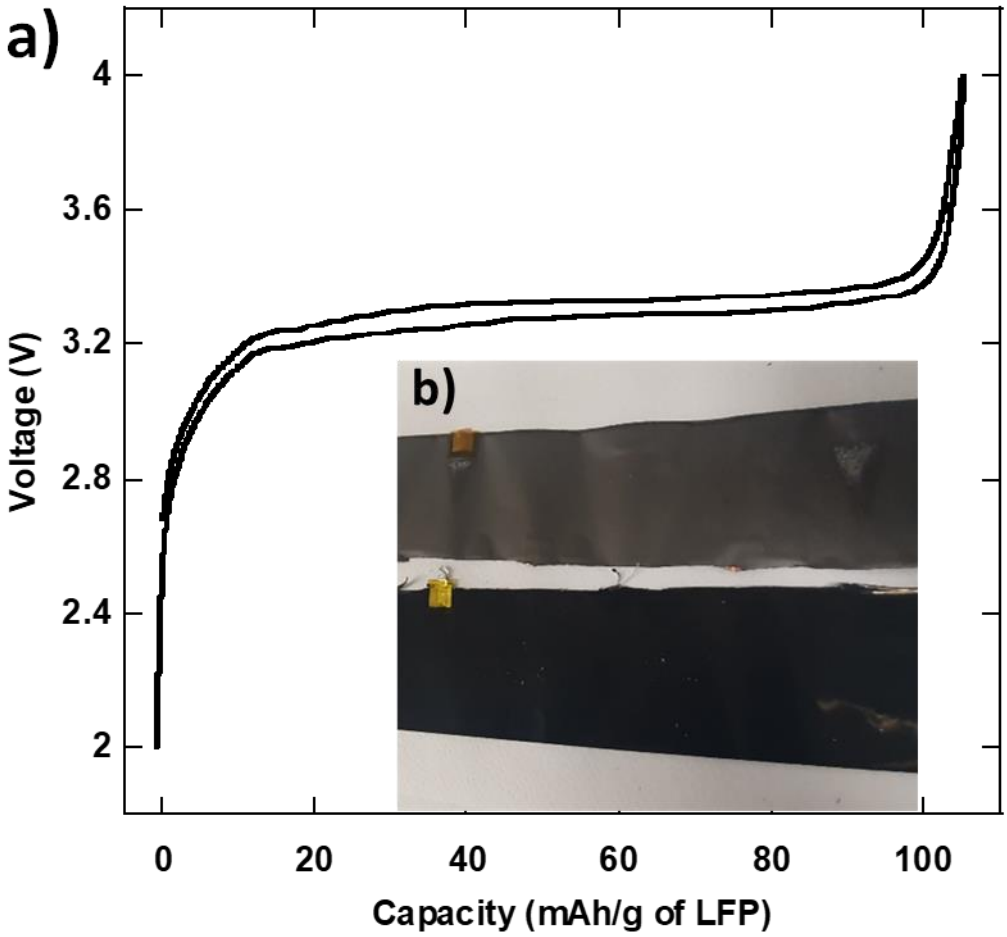

Figure 1

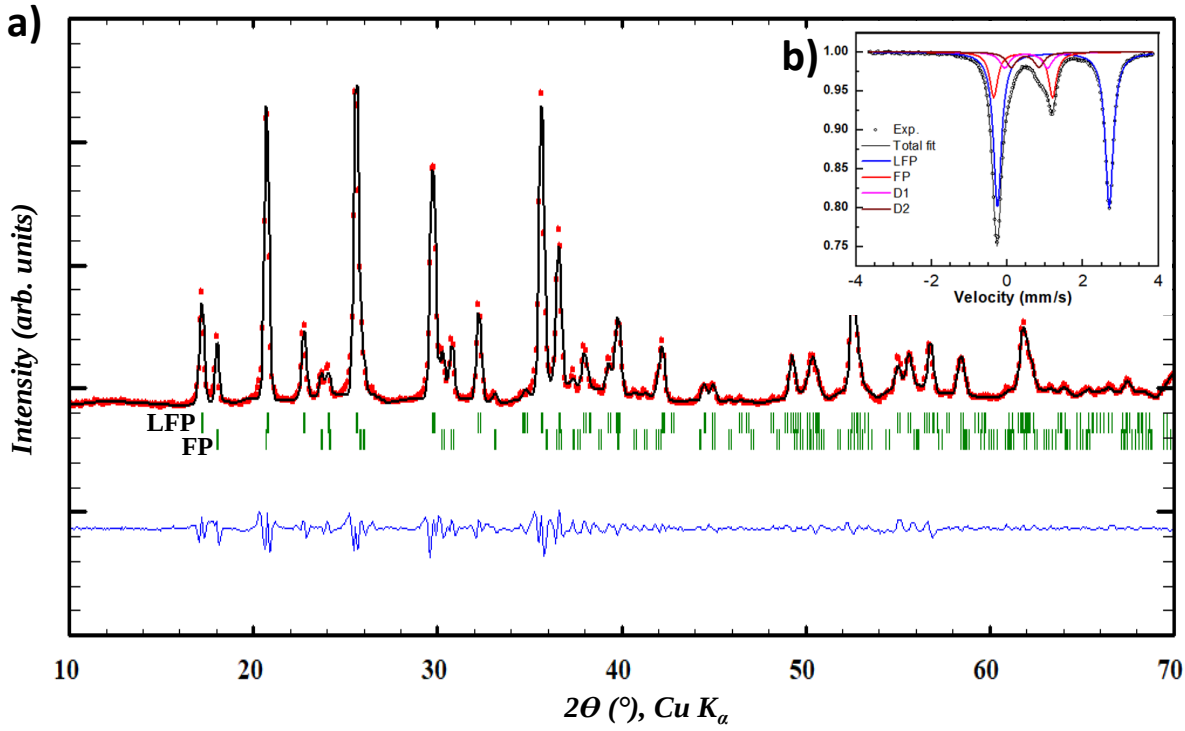
a)
b)
Intensity (arb. units)
LFP
FP
10
20
30
40
50
60
70
2Θ (°), Cu K$_\alpha$
1.00
0.95
0.90
0.85
0.80
0.75
Exp.
Total fit
LFP
FP
D1
D2
-4
-2
0
2
4
Velocity (mm/s)

Figure 2

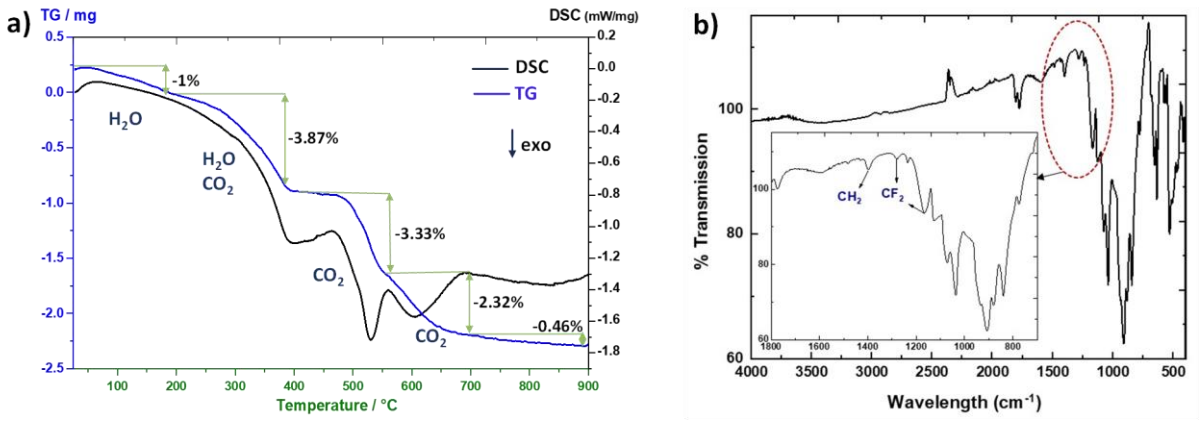
a)
TG / mg
DSC (mW/mg)
DSC
TG
exo
-1%
-3.87%
-3.33%
-2.32%
-0.46%
H2O
H2O
CO2
CO2
CO2
Temperature / °C
b)
% Transmission
Wavelength (cm-1)
CH2
CF2

Figure 3

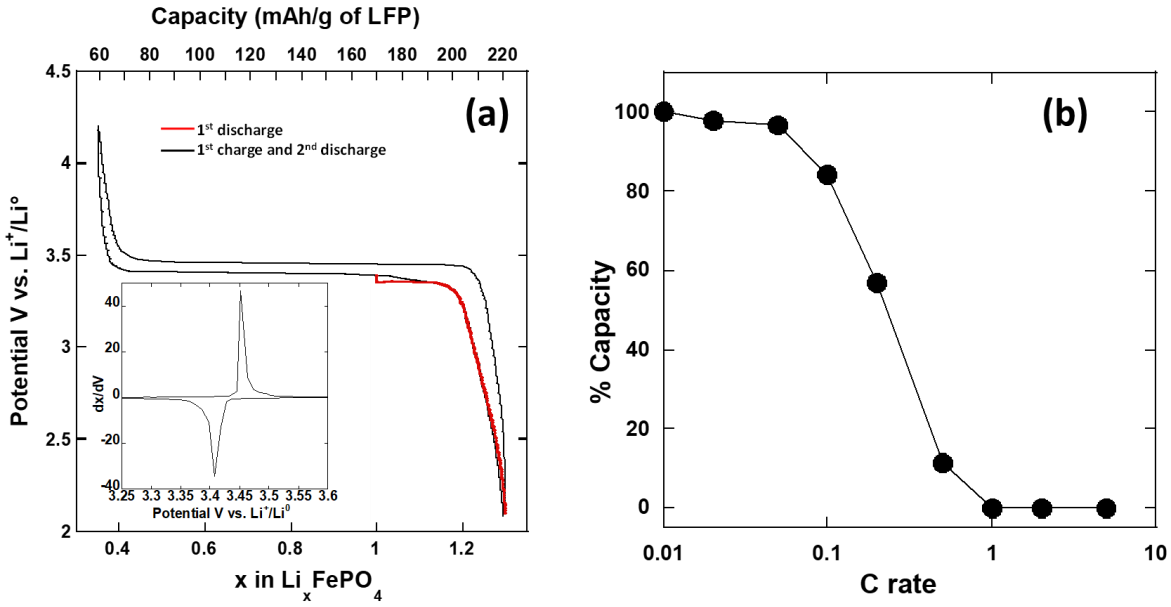
Capacity (mAh/g of LFP)
60 80 100 120 140 160 180 200 220
4.5 4 3.5 3 2.5 2
(a)
1st discharge
1st charge and 2nd discharge
Potential V vs. Li+/Li°
dx/dV
40 20 0 -20 -40
3.25 3.3 3.35 3.4 3.45 3.5 3.55 3.6
Potential V vs. Li+/Li0
0.4 0.6 0.8 1 1.2
x in Lix FePO4
(b)
100 80 60 40 20 0
% Capacity
0.01 0.1 1 10
C rate

Figure 4

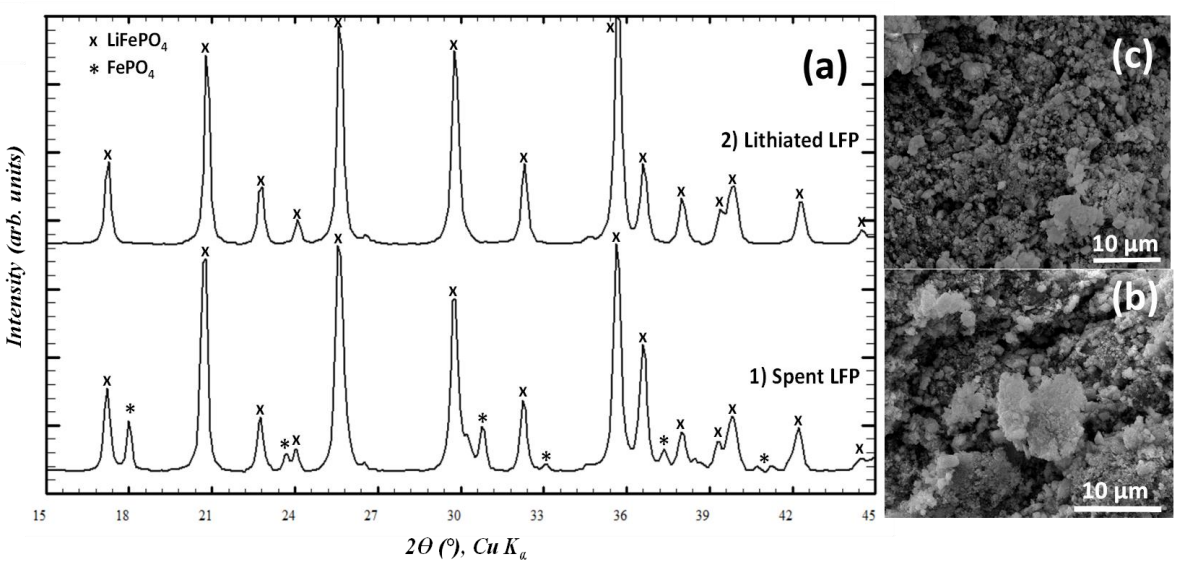
x LiFePO4
* FePO4
(a)
2) Lithiated LFP
1) Spent LFP
Intensity (arb. units)
15
18
21
24
27
30
33
36
39
42
45
2θ (°), Cu Kα
(c)
10 µm
(b)
10 µm

Figure 5

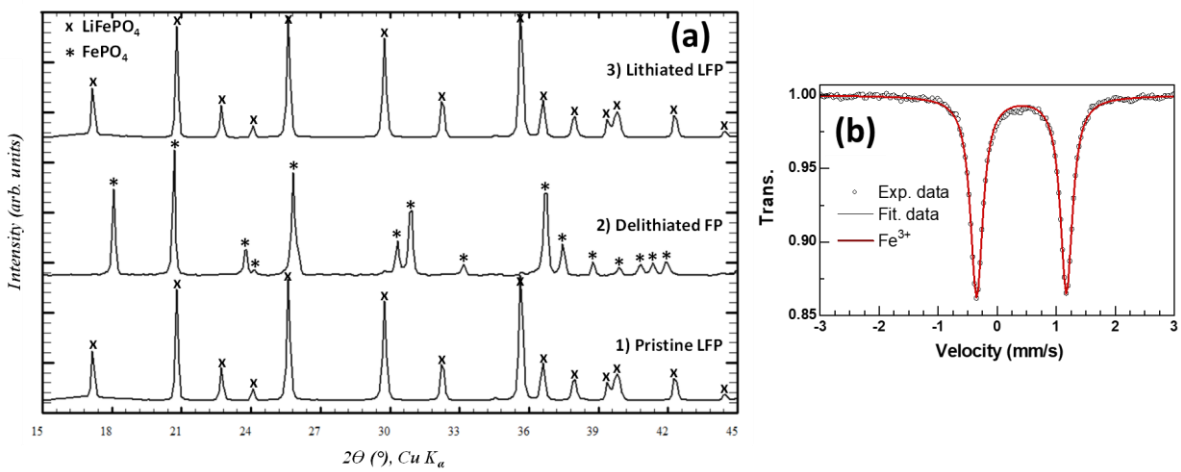
x LiFePO4
* FePO4
(a)
3) Lithiated LFP
2) Delithiated FP
1) Pristine LFP
Intensity (arb. units)
2θ (°), Cu Kα
15
18
21
24
27
30
33
36
39
42
45
(b)
Exp. data
Fit. data
Fe3+
Trans.
Velocity (mm/s)
1.00
0.95
0.90
0.85
-3
-2
-1
0
1
2
3

Figure 6

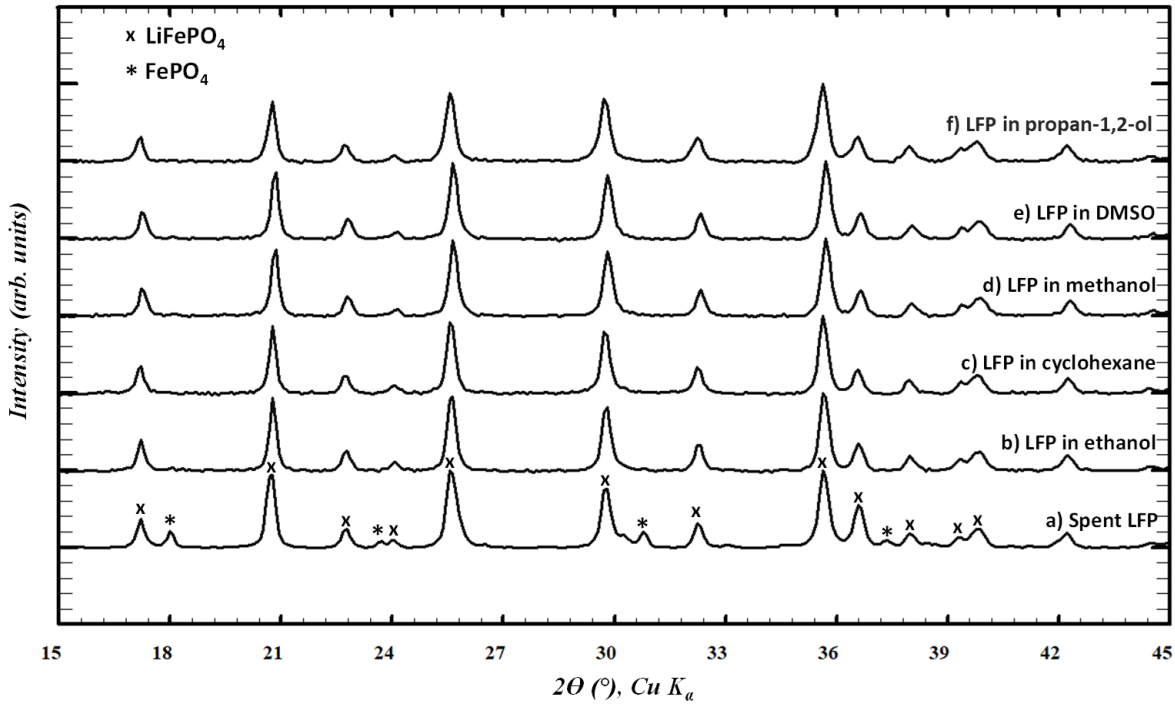
x LiFePO4
* FePO4
f) LFP in propan-1,2-ol
e) LFP in DMSO
d) LFP in methanol
c) LFP in cyclohexane
b) LFP in ethanol
a) Spent LFP
Intensity (arb. units)
15
18
21
24
27
30
33
36
39
42
45
2Θ (°), Cu Kα

Figure 7

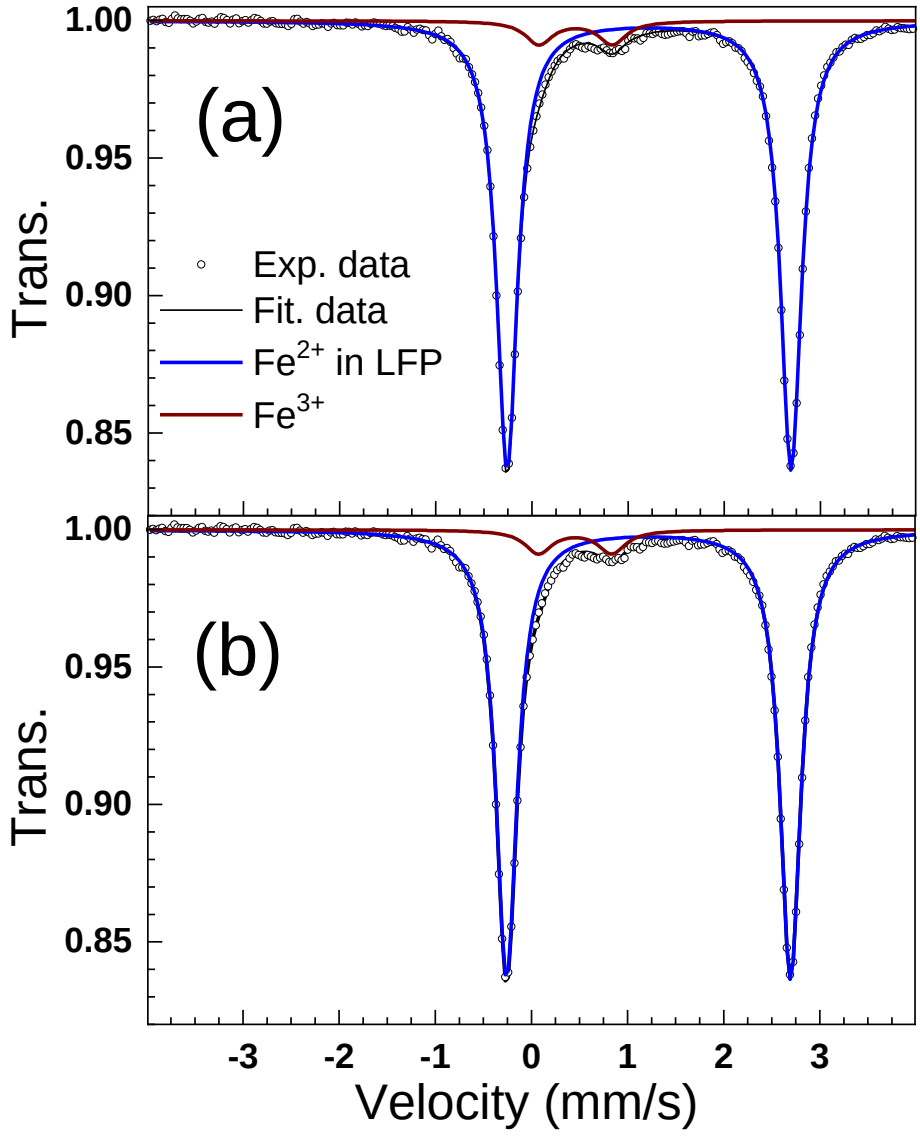
(a)
(b)
Exp. data
Fit. data
Fe2+ in LFP
Fe3+
Trans.
Trans.
1.00
0.95
0.90
0.85
1.00
0.95
0.90
0.85
-3
-2
-1
0
1
2
3
Velocity (mm/s)

Figure 8

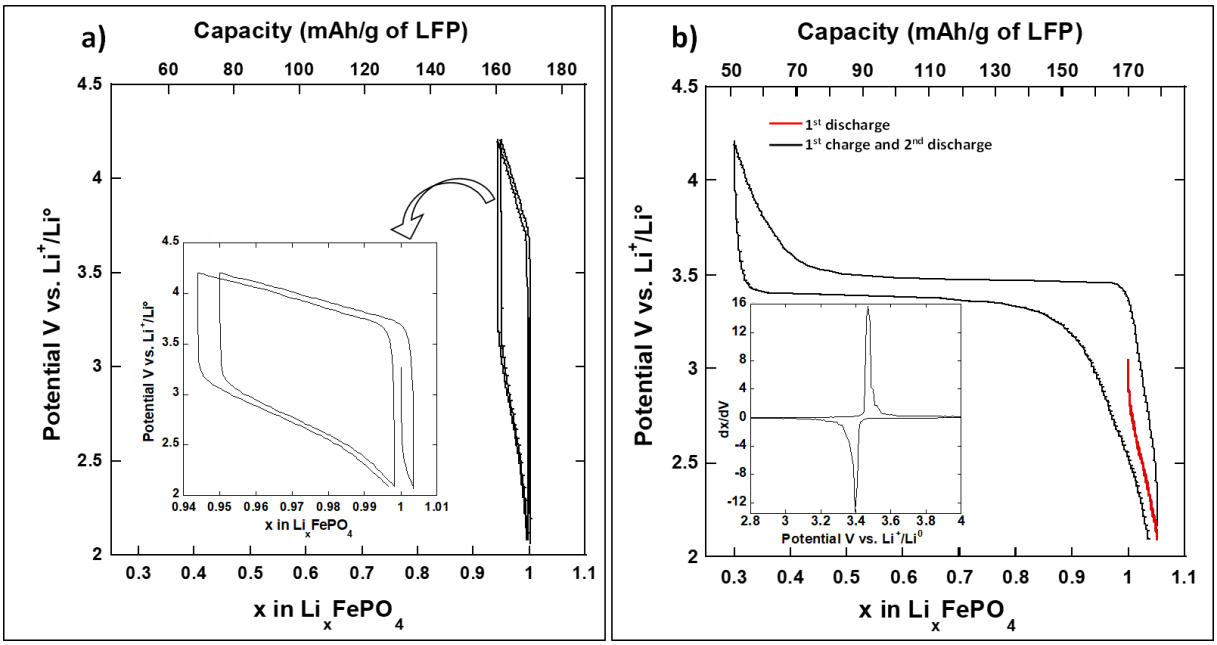
a)
Capacity (mAh/g of LFP)
60 80 100 120 140 160 180
4.5 4 3.5 3 2.5 2
Potential V vs. Li+/Li°
0.3 0.4 0.5 0.6 0.7 0.8 0.9 1 1.1
x in Lix FePO4
Potential V vs. Li+/Li°
4.5 4 3.5 3 2.5 2
0.94 0.95 0.96 0.97 0.98 0.99 1 1.01
x in Lix FePO4
b)
Capacity (mAh/g of LFP)
50 70 90 110 130 150 170
1st discharge
1st charge and 2nd discharge
Potential V vs. Li+/Li°
4.5 4 3.5 3 2.5 2
dx/dV
16 12 8 4 0 -4 -8 -12
2.8 3 3.2 3.4 3.6 3.8 4
Potential V vs. Li+/Li0
0.3 0.4 0.5 0.6 0.7 0.8 0.9 1 1.1
x in Lix FePO4

Figure 9

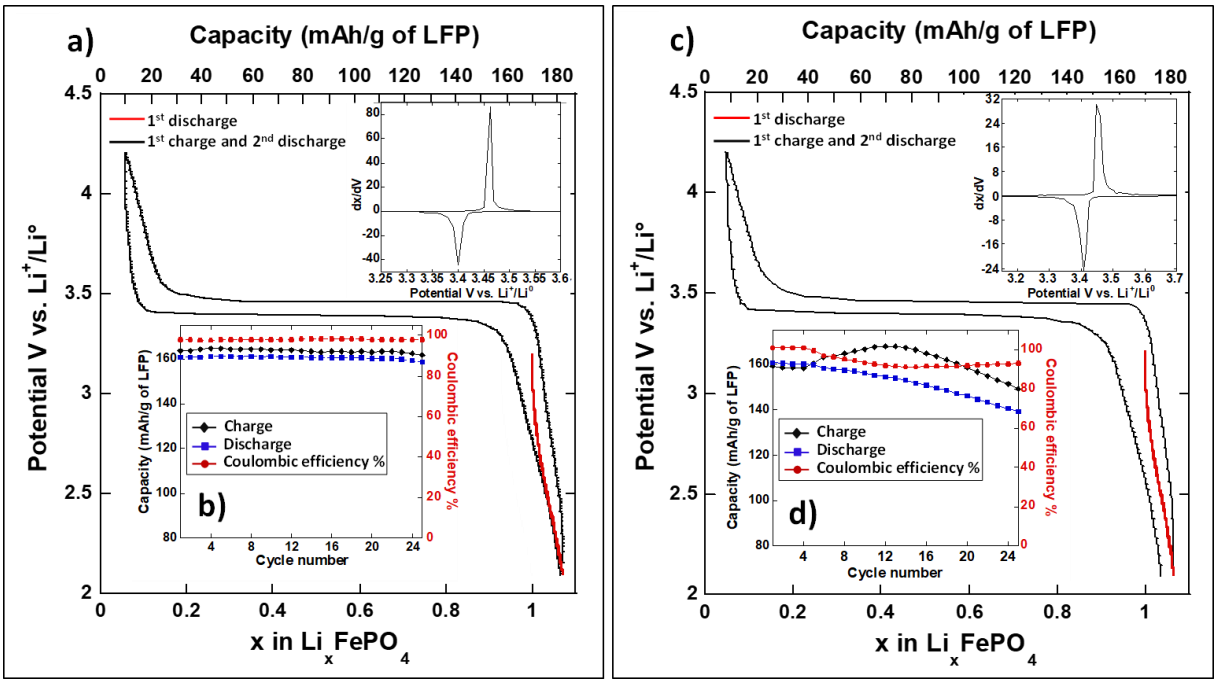
a)
Capacity (mAh/g of LFP)
1st discharge
1st charge and 2nd discharge
Potential V vs. Li+/Li°
x in Li x FePO 4
dx/dV
Potential V vs. Li+/Li°
b)
Charge
Discharge
Coulombic efficiency %
Capacity (mAh/g of LFP)
Coulombic efficiency %
Cycle number
c)
Capacity (mAh/g of LFP)
1st discharge
1st charge and 2nd discharge
Potential V vs. Li+/Li°
x in Li x FePO 4
dx/dV
Potential V vs. Li+/Li°
d)
Charge
Discharge
Coulombic efficiency %
Capacity (mAh/g of LFP)
Coulombic efficiency %
Cycle number

Figure 10

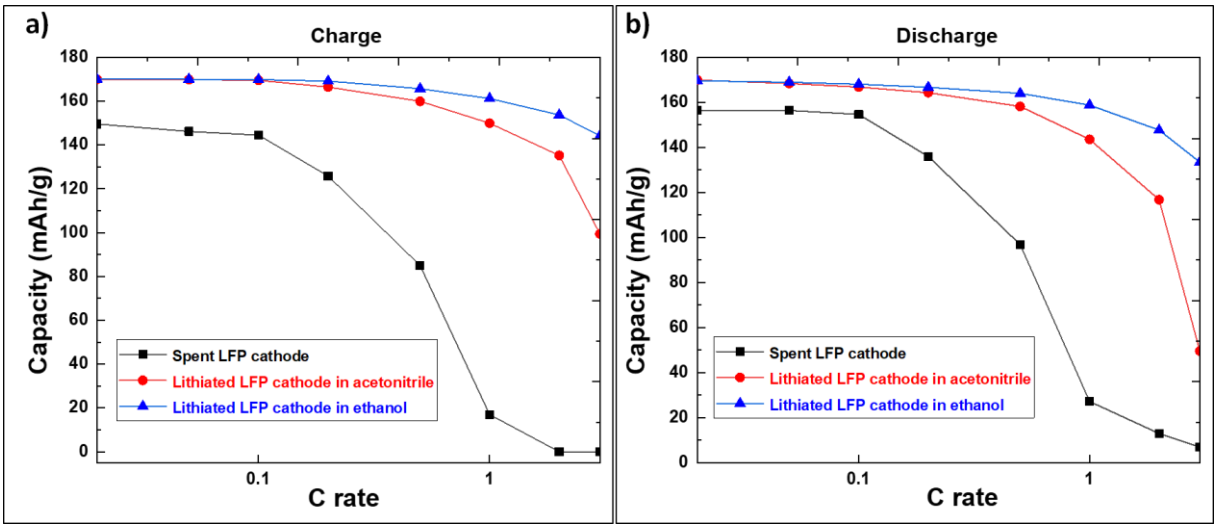
a)
Charge
Capacity (mAh/g)
C rate
Spent LFP cathode
Lithiated LFP cathode in acetonitrile
Lithiated LFP cathode in ethanol
b)
Discharge
Capacity (mAh/g)
C rate
Spent LFP cathode
Lithiated LFP cathode in acetonitrile
Lithiated LFP cathode in ethanol

Figure 11